Complex free-energy landscapes in biaxial nematic liquid crystals and the role of repulsive interactions: A Wang-Landau study

B. Kamala Latha,[1,*] K. P. N. Murthy,[1,†] and V. S. S. Sastry[1,2]
[1]*School of Physics, University of Hyderabad, Hyderabad 500046, India*
[2]*Centre for Modelling, Simulation and Design, University of Hyderabad, Hyderabad 500046, India*
(Received 16 June 2017; published 22 September 2017)

General quadratic Hamiltonian models, describing the interaction between liquid-crystal molecules (typically with D_{2h} symmetry), take into account couplings between their uniaxial and biaxial tensors. While the attractive contributions arising from interactions between similar tensors of the participating molecules provide for eventual condensation of the respective orders at suitably low temperatures, the role of cross coupling between unlike tensors is not fully appreciated. Our recent study with an advanced Monte Carlo technique (entropic sampling) showed clearly the increasing relevance of this cross term in determining the phase diagram (contravening in some regions of model parameter space), the predictions of mean-field theory, and standard Monte Carlo simulation results. In this context, we investigated the phase diagrams and the nature of the phases therein on two trajectories in the parameter space: one is a line in the interior region of biaxial stability believed to be representative of the real systems, and the second is the extensively investigated parabolic path resulting from the London dispersion approximation. In both cases, we find the destabilizing effect of increased cross-coupling interactions, which invariably result in the formation of local biaxial organizations inhomogeneously distributed. This manifests as a small, but unmistakable, contribution of biaxial order in the uniaxial phase. The free-energy profiles computed in the present study as a function of the two dominant order parameters indicate complex landscapes. On the one hand, these profiles account for the unusual thermal behavior of the biaxial order parameter under significant destabilizing influence from the cross terms. On the other, they also allude to the possibility that in real systems, these complexities might indeed be inhibiting the formation of a low-temperature biaxial order itself—perhaps reflecting the difficulties in their ready realization in the laboratory.

DOI: 10.1103/PhysRevE.96.032703

I. INTRODUCTION

The biaxial nematic phase, proposed initially in the work by Freiser and Straley [1,2], has been the subject of many theoretical [3–9] and experimental [10–14] investigations in recent years, and it was investigated extensively via Monte Carlo (MC) simulations [15–24]. However, experimental realization was not so readily possible and is still a matter of debate [25–27].

According to recent mean-field (MF) treatments [28–34], the relevant Hamiltonian parameter space conducive to the formation of a stable biaxial phase is comprised of a triangular region (say, Δ) in the (γ,λ) plane (the essential triangle) shown in Fig. 1 [32], the long axes of the molecules defining the primary director. The quadratic Hamiltonian for the biaxial system adds two more terms to the dominant attractive interaction between the major molecular axes of the neighboring molecules (i.e., the Lebwohl-Lasher interaction term [35]): a coupling between the two molecular biaxial tensors with strength λ, and a cross coupling between the biaxial and uniaxial tensors of the two molecules, through γ. The MF predictions and our earlier MC work [23,24] focused on two specific paths in this plane that have axial symmetry of the torques: along the λ axis (D_{4h} symmetry of molecular pairwise interactions around the molecular z axes), and the diagonal IV (with similar symmetry around the molecular x axes); see Fig. 1. The deviations from the MF work become discernible when γ is appreciable, with the corresponding interactions competing with those of λ, along the path IV (Fig. 1). Earlier MC simulations based on standard METROPOLIS sampling methods [34], while being generally supportive of MF results, were qualitatively deviating from our MC data, obtained through entropic sampling methods. We reported an additional intermediate biaxial phase in the MF predicted direct (N_B-I) transition sequence, starting from the point K and extending up to the point V encompassing the Landau point T [24]. T is special since it represents a pure biaxial interaction between the two major axes (y and z) with D_{4h} pair-interaction symmetry and with no uniaxial coupling between the minor axes (x axes). Incidentally, it also represents a crossover point on the dispersion parabola (OT) from the prolate to oblate molecular symmetry.

The more realistic choices for (γ,λ) values appear more likely to be within the Δ region, as has been reported experimentally recently [36]. Also of particular interest in the earlier literature are models that correspond to systems satisfying the London dispersion approximation [4,15], reducing the number of independent model parameters to one, with $\lambda = \gamma^2$. The phase diagram along the parabolic trajectory has been extensively studied [17,19], and it has been used as a prototype for several investigations [37–41]. The dispersion parabola also defines an interesting boundary separating regions of (γ,λ) parameter space: one region that makes the Hamiltonian fully attractive above the parabola and the other that makes it partly repulsive (below the parabola) [32]. Investigation of the nature of the phases with entropic sampling techniques as one traverses the parabola from the Lebwohl-Lasher limit (origin)

*kklata@gmail.com
†Present address: Manipal Centre for Natural Sciences, Manipal University, Manipal 576104, India.

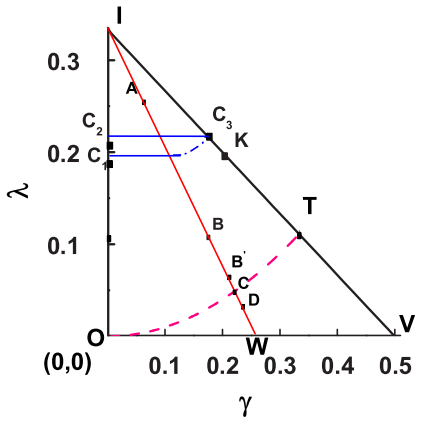

FIG. 1. Essential triangle: Region of biaxial stability. OI and IV are uniaxial torque lines intersecting at the point I. *OCT* is the dispersion parabola which meets line IV at the Landau point T. Base OV is the limit of biaxial stability for the interaction [33]. IW and *OCT* are the trajectories along which present simulations have been carried out. Points A (0.048, 0.269), B (0.166, 0.111), B′ (0.204, 0.061), C (0.215, 0.047) and D (0.225, 0.033) are points of particular interest (see text).

to the Landau point T could be interesting from the standpoint of understanding the destabilizing influence of γ along this path, if any.

In this work, we carried out a detailed entropic sampling-based MC study of the phase diagram on a straight line path within the triangle (IW in Fig. 1), where W is the midpoint of OV. The relative importance of the cross-coupling γ term increases along the path IW, which intersects the parabola at point C, beyond which the γ term provides a repulsive contribution to the Hamiltonian. We supplement these data with results from standard Boltzmann ensembles for comparison. With the density of states obtained from the entropic method, we compute the free-energy profiles as functions of order parameters, with a view to correlating them with the observed thermal behavior of these variables. A similar study was carried out at several points on the parabola. It is interesting to observe the curious changes that the model induces on the macroscopic behavior, as it starts with a small perturbation on the LL model near the origin and moves all the way to the Landau point T. This paper discusses the MC results along these two trajectories.

The paper is divided into five sections. The mean-field Hamiltonian model and its representation for purposes of simulation are outlined in Sec. II. The details of entropic sampling-based simulation are described in Sec. III. The results are presented and discussed in Sec. IV. We summarize the salient features of the work in Sec. V.

II. HAMILTONIAN MODEL

The general interaction between two liquid-crystal molecules with D_{2h} symmetry limited to quadratic terms, each described by two symmetric traceless tensors $(\boldsymbol{q},\boldsymbol{b})$ and $(\boldsymbol{q}',\boldsymbol{b}')$, is expanded as $H = -U[\xi \boldsymbol{q}\cdot\boldsymbol{q}' + \gamma(\boldsymbol{q}\cdot\boldsymbol{b}' + \boldsymbol{q}'\cdot\boldsymbol{b}) + \lambda \boldsymbol{b}\cdot\boldsymbol{b}']$. Here $\boldsymbol{q}$ and $\boldsymbol{b}$ are the irreducible components of the anisotropic parts of the molecular susceptibility tensor, which can be represented in its eigenframe $(\boldsymbol{e},\boldsymbol{e}_\perp,\boldsymbol{m})$ as $\boldsymbol{q} = \boldsymbol{m}\otimes\boldsymbol{m} - \frac{I}{3}$ and $\boldsymbol{b} = \boldsymbol{e}\otimes\boldsymbol{e} - \boldsymbol{e}_\perp\otimes\boldsymbol{e}_\perp$. Similar representation (for a neighboring molecule) holds for $\boldsymbol{q}'$, $\boldsymbol{b}'$ in the eigenframe $(\boldsymbol{e}',\boldsymbol{e}'_\perp,\boldsymbol{m}')$, following the notation used earlier [28]. MF analysis of the Hamiltonian predicts a triangular region OIV (Fig. 1) [32] as the region of stability for the biaxial phase in the interaction parameter (γ,λ) space, assigning the primary director to the orientation of the long molecular axes. The dispersion parabola $(\lambda = \gamma^2)$ *OCT* divides the parameter space into two regions: the region above within the triangle, *OIT*—where the interaction Hamiltonian is globally attractive, and the one below *OTV*—where the interaction is partly repulsive due to the γ term. The points C_1 and C_3 are tricritical points of the uniaxial nematic-biaxial nematic transition, and C_2 is a triple point hosting the three phases of the medium: isotropic (I), uniaxial nematic (N_U), and biaxial nematic (N_B) [32]. (K is a point where the N_B-I phase sequence has been found to change to N_B-N_{B_1}-I [23], deviating from the MF prediction). MF also predicts a direct N_B-I transition inside the parameter region IC_2C_3, and tricritical nature for the N_U-N_B transition along C_1C_3 [32]. The MF analysis based on the minimax principle involving only the two dominant order parameters (out of the four) permits the existence of a biaxial phase even at the base point V of the triangle $(\lambda = 0)$, though such a phase is forbidden on the grounds of biaxial stability [33].

For the purpose of simulations, the mean-field Hamiltonian is conveniently recast in terms of a biaxial mesogenic lattice model, where two molecules of D_{2h} symmetry at distinct lattice sites, represented by an orthonormal triplet of three-component unit vectors $\boldsymbol{u}_a,\boldsymbol{v}_b$ $(a,b = 1,2,3)$, interact through a nearest-neighbor pair potential [20],

$$U = -\epsilon\{G_{33} - 2\gamma(G_{11} - G_{22}) + \lambda[2(G_{11} + G_{22}) - G_{33}]\}. \quad (1)$$

Here $f_{ab} = (\boldsymbol{u}_a.\boldsymbol{v}_b)$ and $G_{ab} = P_2(f_{ab})$, with P_2 denoting the second Legendre polynomial. ϵ is a positive quantity setting the reduced temperature $T' = k_BT/\epsilon$, where T is the absolute temperature of the system. In these simulations, ϵ is set to unity.

III. DETAILS OF SIMULATION

The Wang-Landau (WL) algorithm [42] addresses the problem of efficient entropic sampling of the configuration space to construct ensembles (in discrete spin systems) that are uniformly distributed with respect to energy through an accurate estimation of the density of states (DOS) of the system. This has been successful in tackling various problems in statistical physics [43,44] as diverse as polymers and protein folding [45–47] and self-assembly [48], and it is being continually updated for application to more complex systems [49–55]. The algorithm was suitably modified for application to systems with continuous degrees of freedom, such as liquid crystals [56], and this procedure is further augmented with the frontier sampling technique [57,58] in order to simulate the bulk biaxial liquid crystal [24]. The WL simulation [42] estimates the DOS, while updating a trial density $g(E)$ iteratively by performing a random walk in the energy space with a probability proportional to the inverse of the instantaneous $g(E)$, until a flat histogram of energy

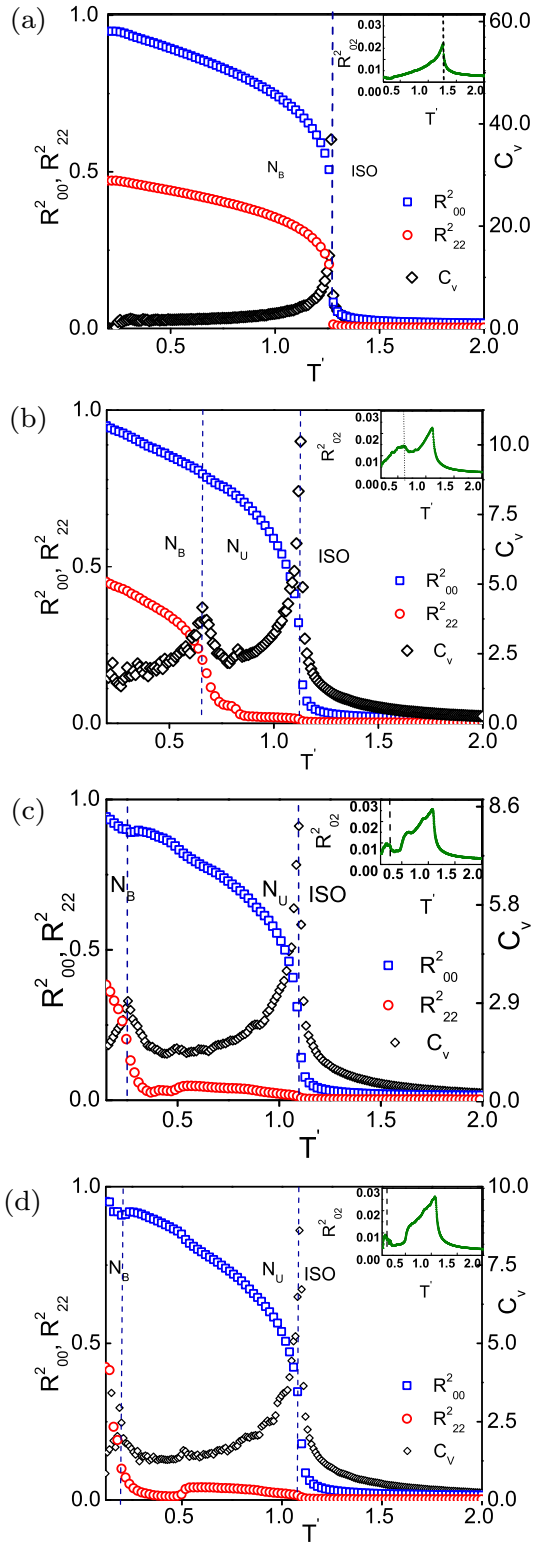

FIG. 2. The temperature variation of order parameters R^2_{00}, R^2_{22} (superimposed on the specific-heat curves) and R^2_{02}(inset) illustrates the phase behavior at the four representative points A, B, C, and D with values of $\lambda' =$ (a) 0.414 (point A), (b) 0.610 (point B), (c) 0.692 (point C), and (d) 0.709 (point D) ($L = 20$).

is achieved as the updating of $g(E)$ is gradually withdrawn. The frontier sampling technique introduces additional algorithmic guidance to the WL routine, so that lower entropic regions are more efficiently accessed. An entropic ensemble of microstates, collected by a random walk guided by the well-converged DOS, is fairly uniformly distributed over the energy region of interest, and it is adequate to calculate the required thermodynamic properties at the desired temperature resolution by constructing equilibrium canonical ensembles (say, RW ensembles) through a reweighting procedure. The free-energy profiles, obtained as a function of energy, and the system order parameters, using the computed DOS, provide further physical insight. We employ here this modified algorithm, described in detail elsewhere [24].

We consider a cubic lattice (size: $L \times L \times L, L = 15,20$) with periodic boundary conditions. The biaxial molecules on each lattice site interact through the nearest-neighbor interaction potential in Eq. (1). The parameters γ and λ are chosen such that we traverse along a trajectory IW passing through the apex I and bisecting the base OV at point W (Fig. 1). The uniaxial-biaxial coupling coefficient γ on IW is half of the value on the diagonal IV for identical λ values. We denote the arclength of the path OIW as λ', given by $\lambda' = \lambda$ on segment OI, and $\lambda' = \frac{1}{3}(1 + 5\gamma)$ where $\gamma = \frac{(1-3\lambda)}{4}$ on the segment IW. As we traverse along the trajectory IW, the arc length λ' varies from $\frac{1}{3}$ at I to 0.75 at W. The simulations are done at various values of λ' on the path IW, starting from the point I ($\lambda' = 1/3$ at $\gamma = 0.0$, $\lambda = 1/3$) and ending at W ($\lambda' = 0.75$ at $\gamma = 0.25$, $\lambda = 0.0$). Points A ($\lambda' = 0.414$ at $\gamma = 0.048$, $\lambda = 0.269$), B ($\lambda' = 0.610$ at $\gamma = 0.166$, $\lambda = 0.111$), and B' ($\lambda' = 0.674$ at $\gamma = 0.204$, $\lambda = 0.061$) lie in the attractive region for the Hamiltonian, while C ($\lambda' = 0.692$ at $\gamma = 0.215$, $\lambda = 0.047$) lies on the dispersion parabola, and D ($\lambda' = 0.709$ at $\gamma = 0.225$, $\lambda = 0.033$) lies in the partly repulsive region, below the parabola.

We start the simulation at a chosen value of λ' with a random orientation of spins on the lattice, and the corresponding values of (γ,λ) are inserted in Eq. (1) for calculating the system energy. An entropic ensemble comprised of ($\sim 4 \times 10^7$) microstates is constructed using the Wang-Landau algorithm, with a fairly uniform distribution of energy at the end of the simulation. Using the computed DOS, canonical ensembles are extracted with the reweighting procedure [59,60] at the chosen temperatures (RW ensembles). Average values of physical variables are then computed at the required temperature resolution. Information on the system energy and the DOS facilitate the determination of free energy as a function of energy as well as order parameters, at different temperatures.

Conventional MC simulations based on the METROPOLIS algorithm (Boltzmann sampling) leading to equilibrium canonical ensembles (B ensembles) were also carried out at chosen points on the trajectory IW in order to compare the results from both simulation methods. These ensembles were collected, after equilibration, with production runs of typically 6×10^5 MC lattice sweeps (Monte Carlo steps). Temperature variations of the equilibrium averages from B and RW ensembles are compared to assess the efficacy of the respective sampling in the presence of curious free-energy terrains in the configuration space offered by the biaxial system.

The physical observables of interest, calculated at each value of λ', are the average energy $\langle E \rangle$, the specific heat $\langle C_v \rangle$, the energy cumulant V_4 [$=1 - \langle E^4 \rangle / (3\langle E^2 \rangle^2)$], which

is a measure of the kurtosis [61], the four order parameters of the phase calculated according to [17,62], and their susceptibilities. These are the uniaxial order $\langle R^2_{00}\rangle$ (along the primary director), the phase biaxiality $\langle R^2_{20}\rangle$, the molecular contribution to the biaxiality of the medium $\langle R^2_{22}\rangle$, and the contribution to uniaxial order from the molecular minor axes $\langle R^2_{02}\rangle$. The averages are computed at a temperature resolution of 0.002 in the temperature (T') range of interest [2.05, 0.05], all in reduced units. The error bars for the observables were estimated after minimizing possible correlations using the jackknife method [63]. The relative errors in the averages of energies are found to be typically one part in 10^5, while those in the estimation of the averages of the order parameters are 1 in 10^4.

IV. RESULTS AND DISCUSSION

We carried out a detailed simulation study employing the entropic sampling technique at 30 values of λ' with a view to obtaining a generic phase diagram inside Δ along IW. We examined the temperature dependence of the C_v profiles, of the two dominant order parameters $\langle R^2_{00}\rangle, \langle R^2_{22}\rangle$ as well as R^2_{02} and the Binder's energy cumulant V_4 to determine the phase-transition temperatures and identify the phases. Typical data such as these at four representative points—at A and B in the fully attractive region, at C on the parabola, and at D in the partly repulsive region (Fig. 1)—are presented in Fig. 2, with a system size $L = 20$ for point A, B, and C and $L = 15$ for point D.

The order profiles superimposed on the specific-heat peaks shown in Fig. 2 indicate that a direct isotropic-biaxial phase transition occurs at point A [Fig. 2(a)]. At all other points, two specific-heat peaks are observed upon cooling, at temperatures T_1 and T_2. As the system is cooled from the isotropic phase, the uniaxial order R^2_{00} shows a sharp increase at T_1, indicating the onset of an intermediate uniaxial phase N_U. It is of interest to note that this intermediate phase also exhibits a small amount of biaxial order, which increases to a value of $\sim$0.03, together with the expected significant increase in the uniaxial order as the temperature decreases. The magnitude of R^2_{22} in this phase seems to be independent of the λ' value in the attractive region (i.e., of the path from I up to C). However, on the bordering trajectory between the two distinct regions of the Hamiltonian (i.e., point C) and in the partly repulsive region (point D), the R^2_{22} value actually dips upon cooling in this intermediate phase after the initial onset [Figs. 2(c) and 2(d)]. The R^2_{22} value then increases rapidly at the second transition (at T_2) for all values of λ', signaling the onset of a low-temperature biaxial phase N_B. Temperature variation of R^2_{02} in each case is shown as an inset [Figs. 2(a)–2(d)].

Based on such study along the trajectory IW, we obtain the phase diagram as a function of the arc length λ', shown in Fig. 3. The actual temperature T' of the simulation needed to be scaled by a factor of 9 [for direct comparison with the Lebwohl-Lasher (LL) model [35]], as $\frac{1}{\beta'} = \frac{T'}{9}$.

Beyond the value of 0.709 of λ', the parameter region presents the dominant cross-coupling term, inducing significant repulsive interactions between the uniaxial and biaxial molecular terms of the neighboring molecules, thus frustrating the system to find a single, stable, and unique free-energy minimum. In this scenario, the computational times for the convergence of the DOS were found to be impractical at this size ($L = 20$). We are thus constrained to report data in this region at $L = 15$.

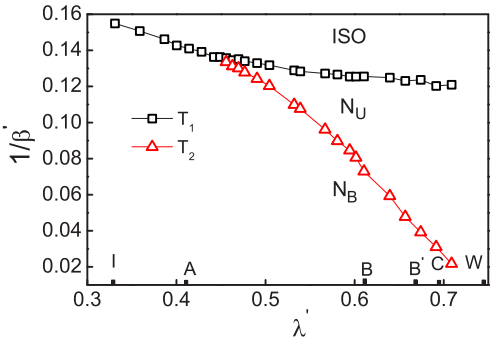

FIG. 3. Phase diagram inside the essential triangle along path IW.

We note from the phase diagram (Fig. 3) that the biaxial medium undergoes a direct I-N_B phase transition for λ' values in the range 1/3–0.455. Thereafter, two transitions were observed in the λ' range 0.462–0.709. The system undergoes an I-N_U transition at high temperature T_1, followed by an N_U-N_B transition at lower temperature T_2. It may be seen that the second transition occurs at progressively lower values of T_2, which approaches zero asymptotically as the point W (on the base OV) is reached, in conformity with the previous MC simulation results in this limit of $\lambda \to 0$ [15].

The nature of the transitions can be gleaned from the plots of the fourth-order energy-cumulant (V_4) data shown in Fig. 4 for some typical values of λ'. The sharp dip in the cumulant value shown in Fig. 4(a) at $\lambda' = 0.345$ is indicative of a strong first-order nature of the N_B-I transition in the λ' range 0.345–0.45. Figures 4(b)–4(d) depict the nature of the two transitions in the range of λ' from 0.463 to 0.692. The I-N_U transition at T_1 shows a progressively weakening first-order nature [relative to Fig. 4(a)], whereas the N_U-N_B transition seems to be continuous over the trajectory. The trajectory in the

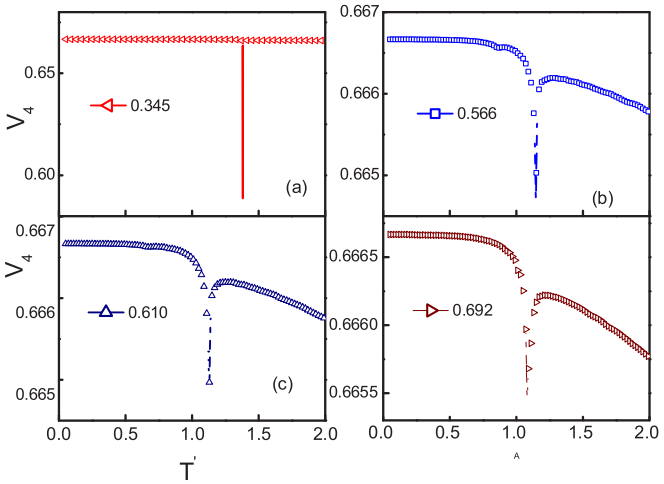

FIG. 4. Energy cumulant V_4 for certain values of λ' in the range 0.345–0.692 (point C).

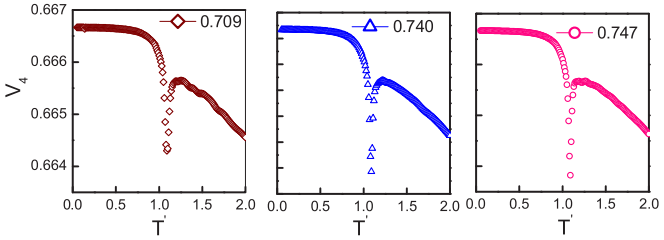

FIG. 5. Energy cumulant V_4 for values of λ' in the range 0.709 (point D) to 0.747 at ($L = 15$).

repulsive region also shows the similar nature of the transitions (Fig. 5).

We computed the equilibrium averages of the observables using B ensembles obtained from MC sampling at randomly chosen points on the trajectory IW. A comparative study of the WL and MC simulation results at four such representative points (at $\lambda' = 0.566$, 0.656, 0.692, and 0.709) are shown in Figs. 6(a)–6(d).

It is observed that qualitative agreement exists between the averages computed from RW and B ensembles up to (and including) $\lambda' = 0.566$. Thereafter, the results vary in the behavior of R^2_{22} in the uniaxial phase. While the B-sampling results point to a pure uniaxial phase (i.e., $R^{22}_{22} \sim 0$ within the error bars) for all values of λ' along the path IW, the RW-sampling results show an unmistakably nonzero and constant value of R^2_{22} ($\sim$0.03) in the uniaxial phase for values of $0.566 < \lambda' \leqslant 0.709$.

We show the representative free energy plotted as a function of energy (per particle) E and the order parameters R^2_{00} and R^2_{22} at $\lambda' = 0.610$ (point B') in the attractive region, in Fig. 7, at different temperatures bracketing the two transition points T_1 and T_2. We observe that the free-energy minima with respect to energy shift toward lower values of energy, while they shift toward higher values of order parameters progressively as the system is cooled. We also note in Fig. 7(c) that the free-energy profile confines the value of R^2_{22} to $\sim$0.03 in the intermediate-temperature region, before allowing its access to higher-order values at the onset of the N_B phase at T_2. Further, the free-energy profile thus confirms that the intermediate phase has to sport in principle a biaxial symmetry, though with a marginal value.

However, as we traverse from this fully attractive region of the Hamiltonian toward the dispersion parabola bordering the repulsive region, the free-energy profiles with respect the biaxial order display curious deviations, and these persist upon entering into the partly repulsive region of the Hamiltonian as well. Figure 8 compares the temperature dependence of free-energy profiles plotted as a function of R^2_{22}, at different points B', C, and D in the triangle (Fig. 1). Temperatures are chosen to represent the profiles in different LC phases. We note from Fig. 8(a) that the free-energy curves at $\lambda' = 0.674$ (point B') show shallow minima at finite values of R^2_{22} (ranging from 0.03 in the N_U phase to 0.24 at the onset of the N_B phase). In contrast, free-energy curves at $\lambda' = 0.692$ [Fig. 8(b) at point C located on the parabola] and 0.709 [Fig. 8(c) at point D, in the partly repulsive region] show a rather curious behavior. We observe that the free energy is a multivalued function of R^2_{22} ($\leqslant$0.04) whenever it shows a nonmonotonic behavior near T_2.

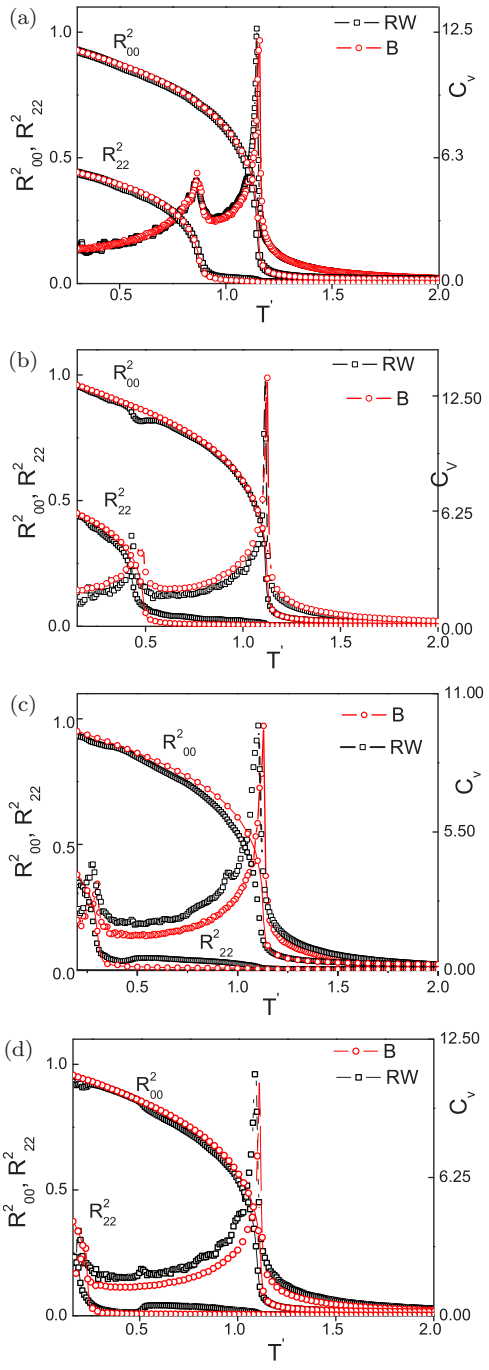

FIG. 6. Comparison of results obtained from RW ensembles (hollow black squares) and B ensembles (hollow red circles). Temperature variation of the specific heat (continuous lines) and the order parameter profiles is shown for four values of λ' along the path IW: (a) 0.566, (b) 0.656, (c) 0.692, and (d) 0.709. It is seen that thermal averages of R^2_{22} from RW ensembles differ from the B ensembles in the intermediate N_U phase for values of $\lambda' > 0.566$.

We interpret this as an indication of the occurrence of distinct sets of plausible microstates with different free energies at the same biaxial order. We also find that the global minimum point of this curve coincides with the thermal equilibrium value of R^2_{22} obtained from a canonical ensemble at the corresponding temperature.

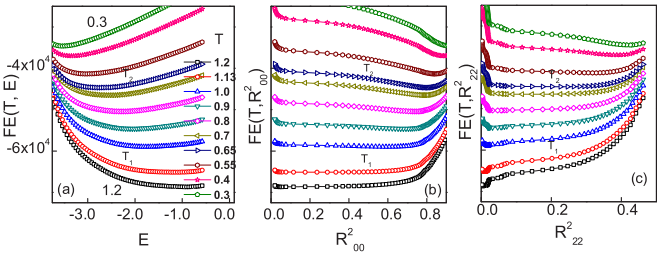

FIG. 7. Free energy shown as a function of (a) energy per particle E, (b) R^2_{00}, and (c) R^2_{22} on cooling from the isotropic phase to the biaxial phase at $\lambda' = 0.610$.

Noting the established accord between the temperature variation of average values of order parameters and the corresponding free-energy profiles in this parameter region, and also keeping in view the observation that the free energy, on the other hand, shows a smooth variation with the energy of the system, the obvious conclusion is that there are subtle changes in the relative contributions of the different orders to the entropy of the system. It seems to show rather pointedly that in the neighborhood of the parabolic boundary, the increased contribution of the cross-coupling term (γ), at the expense of the biaxial-biaxial coupling (λ) attempting to promote macroscopic molecular biaxial order, does not leave the intermediate uniaxial phase in its pristine form (compared to, say, the nematic phase in the LL model or even in the biaxial system on the λ axis, for example). It may be noted that the presence of such inhomogeneous

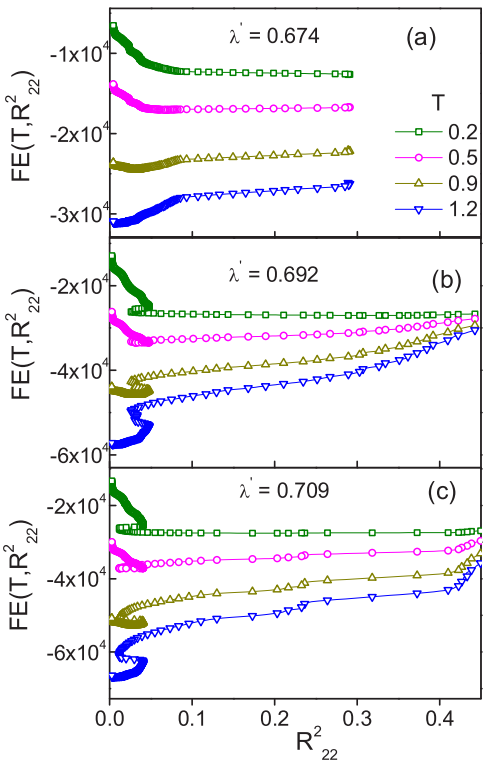

FIG. 8. Representative free energy plotted as a function of R^2_{22} for different values of λ': (a) 0.674, (b) 0.692, and (c) 0.709 [$L = 20$ for (a) and (b) and $L = 15$ for (c)].

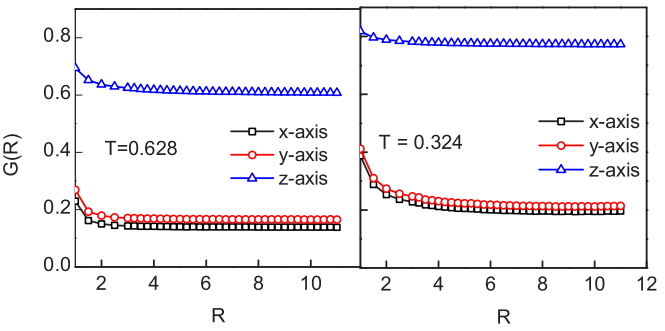

FIG. 9. Correlation function $G(r)$ of x, y, and z molecular axes plotted as a function of the distance r at the point C ($\lambda' = 0.692$) at two temperatures in the N_U phase.

structures and their contribution to the macroscopic averages of order have been investigated, and the presence of "clusters" was alluded to, in the biaxial cluster model of nematics by Vanakaras [64,65] (which was proposed to explain the recent experimental observation of phase biaxiality in bent-core nematics). Indeed, this specific uniaxial phase seems to host local inhomogeneities catering to increased γ contribution and thus shows a nonzero macroscopic R^2_{22} initially originating from such clusters. The subsequent decrease of biaxial order upon further cooling in the uniaxial phase appears to be an indication of the increasing role of the primary order parameter R^2_{00} in effectively contributing to the free-energy minimization in the process, making the system perhaps a more homogeneous uniaxial medium.

Taking advantage of the nonmonotonic variation of R^2_{22} within the N_U phase at the point C (on the parabola), we chose two temperature points (0.628 and 0.324) at which the average value of R^2_{22} is the same [Fig. 2(c)]. We collected microstates within a narrow range centered at the corresponding average energy values per site (-2.331 ± 0.001 and -2.784 ± 0.001, respectively), constituting effectively microcanonical ensembles located at the most probable energy values at the respective temperatures. We computed the orientational correlations of different molecular axes with distance (in lattice units) to obtain their spatial correlation functions at the two temperatures. These variations are shown in Fig. 9. Obviously, R^2_{00} has increased significantly over this temperature range and is reflected in the long-range correlation values of the z axes. The minor axes (x and y), however, have qualitatively different decays, flattening to two different plateau values, even though the corresponding macroscopic averages of R^2_{22} are chosen equal. This clearly brings out the subtle differences in the microscopic organization in the two biaxial phases at the two temperatures: the low-temperature phase hosts a higher long-range R^2_{00} order as expected, but interestingly also a relatively higher long-range R^2_{22} order. It may also be seen from the initial decay profiles of the minor axes at the low temperature (Fig. 9) that this hosts biaxial clusters that are correlated over a larger range than their counterparts at the high-temperature point. The low-temperature phase seems to correspond to an emerging homogeneous biaxial phase, homogeneity being perhaps imposed through free-energy considerations, by the inherent degree of the dominant uniaxial order R^2_{00}. The fact that these two temperatures had the same

macroscopic R^2_{22} order, despite having qualitatively differing correlation profiles, also confirms the presence of contributions to R^2_{22} possibly arising from geometrical averages over inhomogeneous regions, at high temperature.

We observe from Figs. 2(c) and 2(d), corresponding to points C and D in Fig. 1, that the discernible dips in R^2_{22} values just above T_2 are also accompanied by sharp increases in the corresponding R^2_{00}. Similarly, a significant increase in R^2_{22} at the subsequent onset of the biaxial phase at T_2 is seen to lead to an abrupt decrease in R^2_{00}, retracing to its original extrapolated value. Interestingly, such complementary rebounds of the two major order parameters are observed only in systems described by regions of parameter space where the repulsive term is dominant, manifesting as inhomogeneous uniaxial media hosting small biaxial clusters. As the energy of the system is found to be a smooth function of T in this region, such curious rebounds should be due to the compulsions imposed on the system arising from free-energy considerations, with temperature switching the relative importance of the ordering and disordering influences of one or the other of the ordering (mean) tensor fields. As was discussed in [66], the ordering effects of the tensor field B [28] coupling to the system at lower temperatures, and thus promoting the ordering of the minor axes, leads also to a rebound of the secondary contribution to the uniaxial order R^2_{02} (along with a small decrease in R^2_{00}), as may be seen in the insets of Fig. 2.

A. Study along the parabolic path OCT

The parabolic path within the triangle extends from the origin O ($\gamma = 0$, $\lambda = 0$, corresponding to the LL model) to the Landau point T ($\gamma = 1/3$, $\lambda = 1/9$), and the interaction parameters are related within the dispersion approximation as $\lambda = \gamma^2$. We carried out an entropic sampling-based MC study at 13 closely spaced points on the parabola (excluding the origin), and we observed that the phase sequence remained the same, I-N_U-N_B, at all points except at T. The Landau point was found to be qualitatively different, hosting two distinct biaxial phases instead, as reported in a recent entropic sampling-based MC study [23,24]. It may be noted that this finding, however, differs from the mean-field prediction [1,3,32] as well as MC results from Boltzmann sampling [17]. The latter studies point to a single low-temperature N_B phase after a direct transition from the isotropic phase. We present the order-parameter profiles at various points on the parabola starting from $\gamma = 0.131$ to $1/3$ in Fig. 10 (at $L = 20$). It is observed from Fig. 10(a) that the biaxial order parameter shows an initial small increase at the onset of the I-N_U transition, followed by a decrease in its value in the deeper uniaxial nematic phase. This anomalous behavior is more pronounced for values of γ ranging from 0.163 to 0.212. The R^2_{22} temperature profiles for γ values in the range 0.245–0.333, on the other hand, increase continuously in the N_U phase [Fig. 10(b)], exhibiting a monotonic behavior. It is observed from both graphs that the temperature range of the uniaxial nematic phase decreases and the biaxial phase appears at progressively higher temperatures as the γ value increases along the parabola. A curious observation from this study is that the intermediate N_U phase is not strictly uniaxial with $R^2_{22} = 0$ (as expected from the earlier studies), but hosts a small degree of biaxial

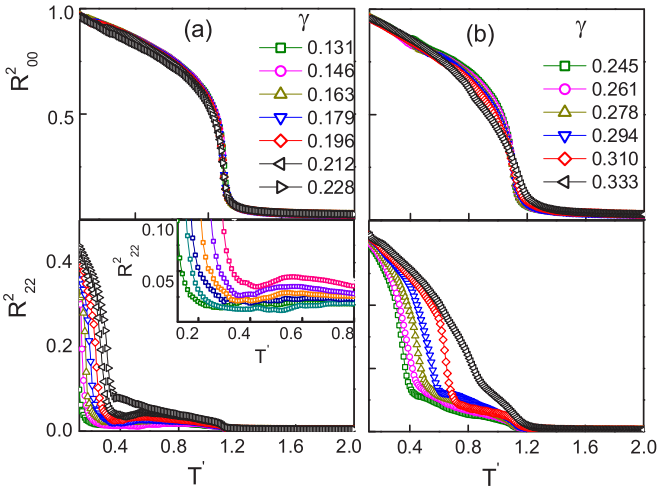

FIG. 10. Uniaxial order (R^2_{00}) and biaxial order (R^2_{22}) plotted as a function of reduced temperature for values of γ ranging from (a) 0.131–0.228 and (b) 0.245–0.333. The inset in (a) shows a magnified version of the R^2_{22} vs T plot where the decrease of R^2_{22} at lower temperatures is seen.

order in the intermediate temperature range. This feature becomes prominent as γ increases beyond ~0.2, indicating the increasingly competing role of the cross-coupling interaction on this very special boundary. The free-energy profiles (plotted against R^2_{22}) shown in Fig. 11 at temperature $T = 0.5$ for values of γ between 0.163 and 0.212 on the parabola show the presence of looplike structures, similar to the earlier observations at point C [Fig. 8(b)], and consistent with the temperature variation of average R^2_{22} values. For higher values of γ (0.228–0.333, Fig. 12), however, these show variations upon cooling, which are in accord with the behavior of R^2_{22} in this region of the parabola.

Thus it emerges that the intermediate N_U phase hosts distinct molecular organizations as the medium is transformed in terms of the symmetry of its molecular interactions from the

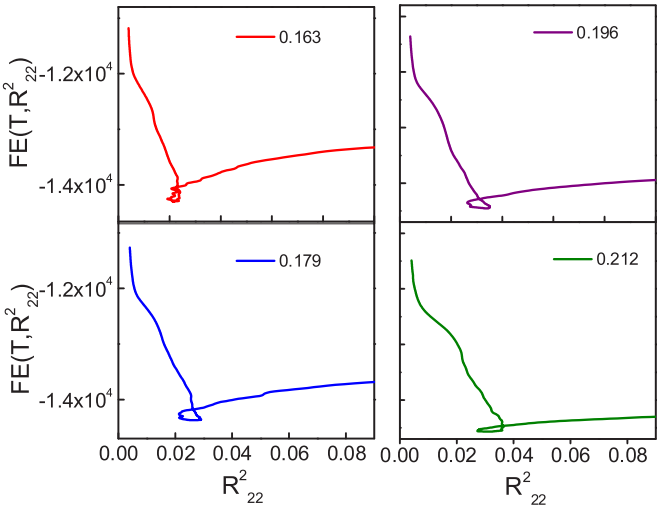

FIG. 11. Free energy plotted as a function the biaxial order parameter R^2_{22} for four values of γ in the neighborhood of point C (including C, $\gamma = 0.212$).

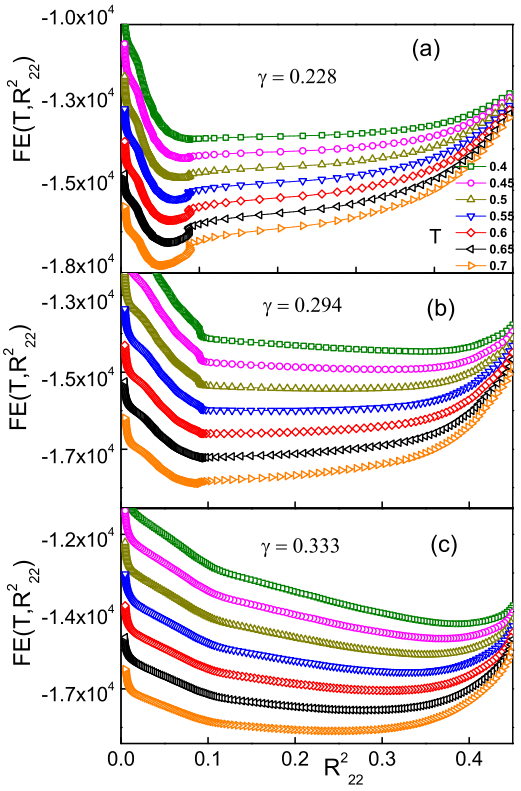

FIG. 12. Free energy shown as a function of R^2_{22}, on cooling in the uniaxial nematic phase for values of (a) $\gamma = 0.228$, (b) $\gamma = 0.294$, and (c) $\gamma = 0.333$.

LL model to the Landau point along the parabola. Discernible degree of biaxial order and its curious temperature variations along the path starting from the origin (LL model) hint at the possibility that the parabola is in fact a very special trajectory having differing types of N_U phases as the Landau point is reached. The parabola serves as an interesting boundary between distinct natures of the Hamiltonian, and it transforms the system interaction symmetry while simultaneously promoting the influence of the cross-coupling terms as one moves from the LL limit. Obviously the nonmonotonic temperature dependence of R^2_{22} is associated with the complex free-energy terrain exhibited by the system in the R^2_{00}-R^2_{22} space, originating from an increasing degree of the cross-coupling term. Viewed from this perspective, the present data provide an insight into the role of γ and λ as their relative importance changes on this trajectory.

V. CONCLUSIONS

We report the results of detailed MC simulations (based on the Wang-Landau technique) along two trajectories inside the triangle Δ. In the first case, along the line IW, we find that our results are in accord with MF predictions in terms of the phase sequences expected. We observe, however, that as we progressively move toward the base point W, in the process changing the relative importance of γ and λ terms in Eq. (1), the uniaxial phase develops a marginal degree of biaxial order R^2_{22} that is sustained through the uniaxial range. This is similar to our earlier observation on the diagonal IV as one progressively traverses toward V [23,24]. The onset of a biaxial phase with significant order at the low-temperature transition is preceded by a dip in R^2_{22} from its small value ($\sim$0.03).

The trajectory IW encompasses two distinct regions from the point of view of the nature of the Hamiltonian. Up to the point C where IW intersects the dispersion parabola, H is fully attractive. The segment CW corresponds to a partly repulsive region, making the stability of the biaxial phase untenable asymptotically as the point W is reached. We make use of the DOS estimates in our simulation to plot the free-energy profiles as a function of the order parameters (R^2_{00}, R^2_{22}) as well as the energy. The observed interesting temperature variation of R^2_{22} within the "uniaxial" phase is consistent with the requirements of the free-energy profiles at different λ' values along the trajectory.

The parabolic trajectory *OCT*, very well studied earlier for its simplifying dispersion approximation, is revisited with the present MC technique to examine if the intermediate uniaxial phase retains its pristine symmetry ($R^2_{22} = 0$ in this phase) throughout its path. The present data indicate that the intermediate uniaxial phase exhibits a small degree of biaxial order as γ increases, and as the Landau point is reached it indeed seems to transform into a biaxial phase in its own right [23,24].

The appearance of a small degree of biaxial symmetry within the uniaxial phase, whenever γ assumes a dominant role, has its origin in the presence of local biaxial inhomogeneities (referred to as "clusters" in [64,65]). Their formation and sustenance is facilitated by the corresponding cross-coupling interaction, which eventually interferes with the homogeneous onset of the two orders. This inference may well have implications in the observed difficulties in realizing readily a biaxial phase in the laboratory.

ACKNOWLEDGMENTS

We wish to thank Shri Singh, Department of Physics, Banaras Hindu University and Surajit Dhara, School of Physics, University of Hyderabad for useful discussions. These simulations were carried out in the Centre for Modelling, Simulation and Design (CMSD) at the University of Hyderabad. BKL acknowledges financial support from Department of Science and Technology (DST), Government of India vide Grant No. SR/WOS-A/PM-2/2016 to carry out this work.

[1] M. J. Freiser, Phys. Rev. Lett. **24**, 1041 (1970).
[2] J. P. Straley, Phys. Rev. A **10**, 1881 (1974).
[3] R. Alben, Phys. Rev. Lett. **30**, 778 (1973).
[4] G. R. Luckhurst, C. Zannoni, P. L. Nordio, and U. Segre, Mol. Phys. **30**, 1345 (1975).
[5] N. Bocara, R. Mejdani, and L. De Seze, J. Phys. (Paris) **38**, 149 (1976).

[6] E. F. Gramsbergen, L. Longa, and W. H. de Jeu, Phys. Rep. **135**, 195 (1986).
[7] D. K. Remler and A. D. J. Haymet, J. Phys. Chem. **90**, 5426 (1986).
[8] B. Mulder, Phys. Rev. A **39**, 360 (1989).
[9] P. I. C. Teixeira, A. J. Masters, and B. M. Mulder, Mol. Cryst. Liq. Cryst. Sci. Technol., Sect. A **323**, 167 (1998).
[10] B. R. Acharya, A. Primak, and S. Kumar, Phys. Rev. Lett. **92**, 145506 (2004).
[11] L. A. Madsen, T. J. Dingemans, M. Nakata, and E. T. Samulski, Phys. Rev. Lett. **92**, 145505 (2004).
[12] K. Merkel, A. Kocot, J. K. Vij, R. Korlacki, G. H. Mehl, and T. Meyer, Phys. Rev. Lett. **93**, 237801 (2004).
[13] J. L. Figueirinhas, C. Cruz, D. Filip, G. Feio, A. C. Ribeiro, Y. Frere, T. Meyer, and G. H. Mehl, Phys. Rev. Lett. **94**, 107802 (2005).
[14] K. Severing and K. Saalwachter, Phys. Rev. Lett. **92**, 125501 (2004).
[15] G. R. Luckhurst and S. Romano, Mol. Phys. **40**, 129 (1980).
[16] M. P. Allen, Liq. Cryst. **8**, 499 (1990).
[17] F. Biscarini, C. Chiccoli, P. Pasini, F. Semeria, and C. Zannoni, Phys. Rev. Lett. **75**, 1803 (1995).
[18] P. J. Camp and M. P. Allen, J. Chem. Phys. **106**, 6681 (1997).
[19] C. Chiccoli, P. Pasini, F. Semeria, and C. Zannoni, Int. J. Mod. Phys. C **10**, 469 (1999).
[20] S. Romano, Physica A **337**, 505 (2004).
[21] S. Romano, Physica A **339**, 511 (2004).
[22] G. Sai Preeti, K. P. N. Murthy, V. S. S. Sastry, C. Chiccoli, P. Pasini, R. Berardi, and C. Zannoni, Soft Matter **7**, 11483 (2011).
[23] B. Kamala Latha, R. Jose, K. P. N. Murthy, and V. S. S. Sastry, Phys. Rev. E **89**, 050501(R) (2014).
[24] B. Kamala Latha, R. Jose, K. P. N. Murthy, and V. S. S. Sastry, Phys. Rev. E **92**, 012505 (2015).
[25] K. Van Le, M. Mathews, M. Chambers, J. Harden, L. Quan, H. Takezoe, and A. Jakli, Phys. Rev. E **79**, 030701(R) (2009).
[26] N. Vaupotic, J. Szydlowska, M. Salamonczyk, A. Kovarova, J. Svoboda, M. Osipov, D. Pociecha, and E. Gorecka, Phys. Rev. E **80**, 030701(R) (2009).
[27] M. Nagaraj, Y. P. Panarin, U. Manna, J. K. Vij, C. Keith, and C. Tschierske, Appl. Phys. Lett. **96**, 0111106 (2010).
[28] A. M. Sonnet, E. G. Virga, and G. E. Durand, Phys. Rev. E **67**, 061701 (2003).
[29] L. Longa, P. Grzybowski, S. Romano, and E. Virga, Phys. Rev. E **71**, 051714 (2005).
[30] G. De Matteis and E. G. Virga, Phys. Rev. E **71**, 061703 (2005).
[31] G. De Matteis, S. Romano, and E. G. Virga, Phys. Rev. E **72**, 041706 (2005).
[32] F. Bisi, E. G. Virga, E. C. Gartland, Jr., G. De Matteis, A. M. Sonnet, and G. E. Durand, Phys. Rev. E **73**, 051709 (2006).
[33] G. De Matteis, F. Bisi, and E. G. Virga, Contin. Mech. Thermodyn. **19**, 1 (2007).
[34] G. De Matteis and S. Romano, Phys. Rev. E **78**, 021702 (2008).
[35] P. A. Lebwohl and G. Lasher, Phys. Rev. A **6**, 426 (1972).
[36] F. Bisi, G. R. Luckhurst, and E. G. Virga, Phys. Rev. E **78**, 021710 (2008).
[37] R. Berardi and C. Zannoni, J. Chem. Phys. **113**, 5971 (2000).
[38] C. Chiccoli, I. Feruli, O. D. Lavrentovich, P. Pasini, S. V. Shiyanovsiccoli, and C. Zannoni, Phys. Rev. E **66**, 030701 (2002).
[39] C. Chiccoli, P. Pasini, I. Feruli, and C. Zannoni, Mol. Cryst. Liq. Cryst. **441**, 319 (2005).
[40] R. Berardi, L. Muccioli, and C. Zannoni, J. Chem. Phys. **128**, 024905 (2008).
[41] R. Berardi, L. Muccioli, S. Orlandi, M. Ricci, and C. Zannoni, J. Phys.: Condens. Matter **20**, 463101 (2008).
[42] F. Wang and D. P. Landau, Phys. Rev. Lett. **86**, 2050 (2001); Phys. Rev. E **64**, 056101 (2001).
[43] D. P. Landau and K. Binder, *A Guide to Monte Carlo Simulations in Statistical Physics*, 2nd ed. (Cambridge University Press, Cambridge, 2005).
[44] K. P. N. Murthy, *Monte Carlo Methods in Statistical Physics* (Universities Press, Hyderabad, India, 2004).
[45] N. Rathore, T. A. Knotts, and J. J. de Pablo, Biophys. J. **85**, 3963 (2003).
[46] D. T. Seaton, T. Wust, and D. P. Landau, Phys. Rev. E **81**, 011802 (2010).
[47] P. Singh, S. K. Sarkar, and P. Bandyopadhyay, Chem. Phys. Lett. **514**, 357 (2011).
[48] L. Gai, T. Vogel, K. A. Maerzke, C. R. Lacovella, D. P. Landau, P. T. Cummings, and C. McCabe, J. Chem. Phys. **139**, 054505 (2013).
[49] P. Poulain, F. Calvo, R. Antoine, M. Broyer, and P. Dugourd, Phys. Rev. E **73**, 056704 (2006).
[50] S. Sinha and S. K. Roy, Phys. Lett. A **373**, 308 (2009).
[51] R. Shekhar, J. K. Whitmer, R. Malshe, J. A. Moreno-Razo, T. F. Roberts, and J. J. de Pablo, J. Chem. Phys. **136**, 234503 (2012).
[52] Y. W. Koh and H. K. Lee, Phys. Rev. E **88**, 053302 (2013).
[53] T. Vogel, Y. Wai Li, T. Wust, and D. P. Landau, Phys. Rev. Lett. **110**, 210603 (2013).
[54] K. A. Maerzke, L. Gai, P. T. Cummings, and C. McCabe, J. Phys. Conf. Ser. **487**, 012002 (2014).
[55] Y. L. Xie, P. Chu, Y. L. Wang, J. P. Chen, Z. B. Yan, and J. M. Liu, Phys. Rev. E **89**, 013311 (2014).
[56] D. Jayasri, V. S. S. Sastry, and K. P. N. Murthy, Phys. Rev. E **72**, 036702 (2005).
[57] C. Zhou, T. C. Schulthess, S. Torbrugge, and D. P. Landau, Phys. Rev. Lett. **96**, 120201 (2006).
[58] D. Jayasri, Ph. D. thesis, University of Hyderabad, India (2009).
[59] R. H. Swendsen and J. S. Wang, Phys. Rev. Lett. **58**, 86 (1987).
[60] B. A. Berg, Comput. Phys. Commun. **153**, 397 (2003).
[61] K. Binder, Z. Phys. B **43**, 119 (1981); Phys. Rev. Lett. **47**, 693 (1981).
[62] R. J. Low, Eur. J. Phys. **23**, 111 (2002).
[63] M. E. J. Newman and G. T. Barkema, *Monte Carlo Methods in Statistical Physics* (Clarendon, London, 2002).
[64] A. G. Vanakaras and D. J. Photinos, J. Chem. Phys. **128**, 154512 (2008).
[65] S. D. Peroukidis, P. K. Karahaliou, A. G. Vanakaras, and D. J. Photinos, Liq. Cryst. **36**, 727 (2009).
[66] F. Bisi, S. Romano, and E. G. Virga, Phys. Rev. E **75**, 041705 (2007).